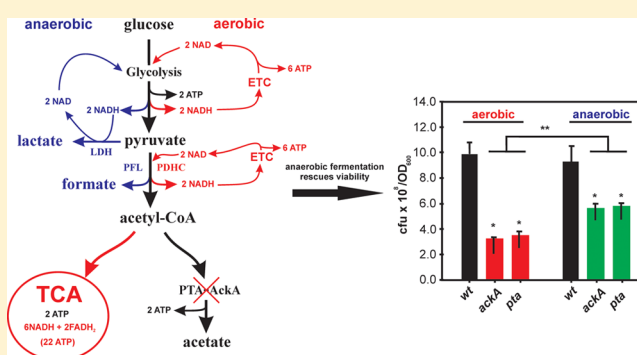


# Redox Imbalance Underlies the Fitness Defect Associated with Inactivation of the Pta-AckA Pathway in *Staphylococcus aureus*

Darrell D. Marshall,<sup>†</sup> Marat R. Sadykov,<sup>‡</sup> Vinai C. Thomas,<sup>‡</sup> Kenneth W. Bayles,<sup>‡</sup> and Robert Powers<sup>\*,†</sup><sup>†</sup>Department of Chemistry, University of Nebraska-Lincoln, Lincoln, Nebraska 68588, United States<sup>‡</sup>Department of Pathology and Microbiology, University of Nebraska Medical Center, Omaha, Nebraska 68198, United States**S** Supporting Information

**ABSTRACT:** The phosphotransacetylase-acetate kinase (Pta-AckA) pathway is thought to be a vital ATP generating pathway for *Staphylococcus aureus*. Disruption of the Pta-AckA pathway during overflow metabolism causes significant reduction in growth rate and viability, albeit not due to intracellular ATP depletion. Here, we demonstrate that toxicity associated with inactivation of the Pta-AckA pathway resulted from an altered intracellular redox environment. Growth of the *pta* and *ackA* mutants under anaerobic conditions partially restored cell viability. NMR metabolomics analyses and <sup>13</sup>C<sub>6</sub>-glucose metabolism tracing experiments revealed the activity of multiple pathways that promote redox (NADH/NAD<sup>+</sup>) turnover to be enhanced in the *pta* and *ackA* mutants during anaerobic growth. Restoration of redox homeostasis in the *pta* mutant by overexpressing L- lactate dehydrogenase partially restored its viability under aerobic conditions. Together, our findings suggest that during overflow metabolism, the Pta-AckA pathway plays a critical role in preventing cell viability defects by promoting intracellular redox homeostasis.

**KEYWORDS:** Pta-AckA pathway, metabolomics, redox imbalance, NMR, *Staphylococcus aureus*



## INTRODUCTION

*Staphylococcus aureus* is a versatile human pathogen responsible for a variety of infections that range from folliculitis to life-threatening diseases such as severe sepsis, endocarditis, and bacteremia.<sup>1–3</sup> *S. aureus* infections represent an enormous challenge to physicians because of the emergence and dissemination of multidrug-resistant strains in the health care setting.<sup>1,2</sup> The ability of this bacterial pathogen to survive and efficiently colonize diverse host environments is based on its proficiency to optimize virulence factor production and adjust its metabolism to rapid environmental changes.<sup>4–9</sup>

When grown under aerobic conditions, *S. aureus* primarily metabolizes glucose to acetate through the Pta-AckA pathway. In a recent study, we observed that inactivation of the Pta-AckA pathway resulted in poor growth and reduced viability at the exponential phase. Although carbon flux through the Pta-AckA pathway is used to generate ATP, the aerobic growth and viability defects associated with the *pta* and *ackA* mutants could not have resulted from ATP depletion as these strains surprisingly exhibited increased levels of intracellular ATP, presumably through increased glycolytic flux and redirection of carbon into the TCA cycle.<sup>10</sup> One possibility for the altered growth and viability defects associated with the *pta* and *ackA* mutants may arise from an altered intracellular redox environment resulting from inflated concentrations of NAD<sup>+</sup> and NADH.<sup>10</sup>

In the present study, we address this hypothesis by comparing the growth characteristics and metabolic changes in the *pta* and *ackA* mutants relative to their isogenic wild-type strain following cultivation under aerobic and anaerobic conditions. We demonstrate that although growth defects due to *pta* and *ackA* mutations persisted under both aerobic and anaerobic growth, cell viability relative to the wild-type strain could be partially restored under fermentative growth. Metabolic differences associated with fermentative growth of the *pta* and *ackA* mutants were determined by NMR spectroscopy, and the observed metabolic changes support a role for the normalization of cellular redox status in the restoration of cell viability in the *pta* and *ackA* mutants. Finally, confirming a strong relationship between cellular redox status and cell viability, the increased cell death in the *pta* mutant under aerobic growth could be partially restored to the wild-type levels by increasing NADH turnover following the overexpression of the *ldh1* gene in this mutant.

## MATERIALS AND METHODS

### Bacterial Strains, Plasmids, and Growth Conditions

The construction of the *ackA* and *pta* mutants in *S. aureus* strain UAMS-1 was described previously.<sup>10</sup> The plasmid, pMRS110,

Received: November 30, 2015

Published: March 15, 2016

containing the *ldh1* gene under the control of the cadmium-inducible promoter  $P_{cadC}$  was constructed by amplifying 1 kb region from the *S. aureus* UAMS-1 chromosome using the primers, *PstI*-RBS-*ldh1*-f (GTCTCTGCAGCATAAGGAG-GAATTTGTAATGAACAAATTTAAAGGGAACAAAGT) and *ldh1*-r (GGGGTAAGGTTTTACAATTTTTGGAATGG), and inserting the resulting DNA fragment into the *PstI* and *SmaI* sites of the shuttle vector, pBK123.<sup>11</sup>

*S. aureus* strains were grown in tryptic soy broth (TSB) without dextrose (BD Biosciences) supplemented with 0.25% glucose (Sigma-Aldrich) or on TSB containing agar. *S. aureus* cultures for both aerobic and anaerobic conditions were inoculated to 0.06 optical density at 600 nm ( $OD_{600}$ ) units from overnight cultures (grown in TSB without dextrose (BD Biosciences)), incubated at 37 °C, and aerated at 250 rpm with a flask-to-medium ratio of 10:1. Bacterial growth was assessed by measuring the optical density at 600 nm or by determining the number of colony forming units (cfu)  $ml^{-1}$ . Chloramphenicol was purchased from Fisher Scientific and was used at a final concentration of 10  $\mu g/ml$ .

#### Measurement of Extracellular Glucose, Acetic Acid, and D,L-Lactate

Aliquots of bacterial cultures (1 mL) were centrifuged for 3 min at 14 000 rpm at 4 °C. The supernatants were removed and stored at -20 °C until use. Acetate, glucose, and D- and L-lactate concentrations were determined using kits purchased from R-Biopharm according to the manufacturer's protocol.

#### Determination of Intracellular ATP Concentrations

Intracellular ATP concentrations were determined using the BacTiter-Glo kit (Promega). The kit was used according to the manufacturer's directions and as previously described.<sup>10</sup> Metabolite concentrations were normalized to the number of viable-cell counts.

#### NMR Metabolomics Sample Preparation

Samples for one-dimensional (1D)  $^1H$  NMR and two-dimensional (2D)  $^1H$ - $^{13}C$  heteronuclear single quantum coherence (HSQC) experiments were prepared from six and three replicate 50 mL cultures, respectively. *S. aureus* wild-type strain UAMS-1 and mutant strains UAMS-1-*ackA* and UAMS-1-*pta* were grown aerobically or anaerobically in TSB containing 0.25% glucose for 1D  $^1H$  NMR experiments or 0.25% [ $^{13}C_6$ ] glucose (Sigma-Aldrich) for 2D  $^1H$ - $^{13}C$  HSQC experiments. Bacteria (10  $OD_{600}$  units) were harvested during the exponential growth phase (3 h) by centrifugation for 7 min at 4100 rpm at 4 °C and washed with ice cold 50 mM phosphate buffer, pH 7.1. Samples were kept on ice through the entire preparation protocol. Enzymatic activity were quenched by suspending the cells in 700  $\mu L$  of ice-cold ethanol [60% ethanol, 40%  $D_2O$  (Isotec)].<sup>12</sup> The cells were then lysed using lysing matrix B tubes in a FastPrep instrument (Qbiogene). The lysates were centrifuged at 4 °C for 5 min at 14 000 rpm to remove the cell debris. The samples were then lyophilized and suspended in 600  $\mu L$  of 99.8%  $D_2O$  phosphate buffer at pH 7.1 (uncorrected) containing 50 mM of (trimethylsilyl) propionic-2, 2, 3, 3- $D_4$  acid sodium salt (TMSP- $D_4$ ) for 1D  $^1H$  NMR experiments or 500 mM of TMSP- $D_4$  for 2D  $^1H$ - $^{13}C$  HSQC experiments. Samples were then transferred to 5 mm NMR tubes for data collection.

#### NMR Data Collection

1D and 2D NMR data collection and analysis were performed as described previously.<sup>13,14</sup> Briefly, all NMR spectra were

collected on a Bruker Avance DRX 500 MHz spectrometer equipped with a 5 mm triple-resonance ( $^1H$ ,  $^{13}C$ ,  $^{15}N$ ), Z-axis gradient cryoprobe. Automated data collection utilized a Bruker ATM unit for automatic tuning and matching, a BACS-120 sample changer and Bruker Icon NMR software. The 1D  $^1H$  NMR spectra were collected using excitation sculpting for water suppression.<sup>15</sup> The 1D  $^1H$  NMR spectra were acquired at 298.15 K with 128 scans, 16 K data points, 16 dummy scans, a relaxation delay of 1.5 s, a spectral width of 5000 Hz, and a total acquisition time of approximately 7 min. 2D  $^1H$ - $^{13}C$  HSQC NMR spectra were collected at 298.15 K with 128 scans and a relaxation delay of 1.5 s. The spectra were collected with 2K data points and a spectrum width of 5000 Hz in the direct dimension, 64 data points and a spectrum width of 17 605.6 Hz in the indirect dimension, and a total acquisition time of approximately 4 h. The 2D  $^1H$ - $^{13}C$  HSQC NMR spectra were processed in NMRPipe and analyzed with NMRViewJ version 9.<sup>16,17</sup>

#### Multivariate Statistical Analysis

The 1D  $^1H$  NMR spectra were processed in our MVAPACK software suite (<http://bionmr.unl.edu/mvapack.php>).<sup>18</sup> For principal component analysis (PCA) and orthogonal projections to latent structures discriminant analysis (OPLS-DA), all spectra were processed with a 1.0 Hz exponential apodization function prior to being Fourier transformed, automatically phased and normalized using our phase-scatter correction (PSC),<sup>19</sup> referenced to TMSP- $D_4$  (0.0 ppm), and scaled using Pareto scaling. For PCA, spectra were binned using an adaptive intelligent binning algorithm that minimizes splitting signals between multiple bins.<sup>20</sup> Spectral regions containing noise or solvent signals were removed manually.<sup>21</sup> For OPLS-DA, full-resolution spectra were used to build the model after alignment with the icoshift algorithm<sup>22</sup> implemented in MVAPACK. OPLS-DA models were calculated using one predictive and one orthogonal component and were cross-validated using a Monte Carlo leave-*n*-out (MCCV) procedure.<sup>23</sup> The  $R^2_y$  (degree of fit) and  $Q^2$  (predictive ability) metrics of 0.99236 and 0.97135 for UAMS-1, 0.98905 and 0.96931 for UAMS-1-*ackA*, and 0.95065 and 0.87454 for the UAMS-1-*pta*, respectively, indicated high-quality OPLS-DA models. Model validation by CV-ANOVA<sup>24</sup> indicated reliable models with *p* values of  $3.1 \times 10^{-3}$ ,  $2.6 \times 10^{-4}$ , and  $7.3 \times 10^{-5}$  for the UAMS-1, UAMS-1-*ackA*, and UAMS-1-*pta* data, respectively. For all strain comparisons, response permutation tests for OPLS-DA model validation also returned *p* values of less than 0.01. The OPLS-DA scores plots and back-scaled loadings were calculated using the entire NMR spectrum (no binning). In this manner, the back-scaled loadings plot resembles a traditional 1D  $^1H$  NMR spectrum, in which peaks (metabolites) abundant under anaerobic conditions are positive and peaks (metabolites) abundant under aerobic conditions are negative.

#### Metabolite Identification

The metabolites significantly contributing to class separation in the OPLS-DA scores plot were identified using the Chenomx NMR Suite 8.0. Simply, the experimental 1D  $^1H$  NMR spectra were assigned using the Chenomx software and then the back-scaled loadings plot was overlaid with the assigned 1D  $^1H$  NMR spectrum to assign the major features in the back-scaled loadings plot.

Metabolite identification using 2D NMR data sets was performed as described previously.<sup>13,14</sup> Briefly, the 2D  $^1H$ - $^{13}C$  HSQC NMR spectra were referenced to TMSP- $D_4$ , and lists of

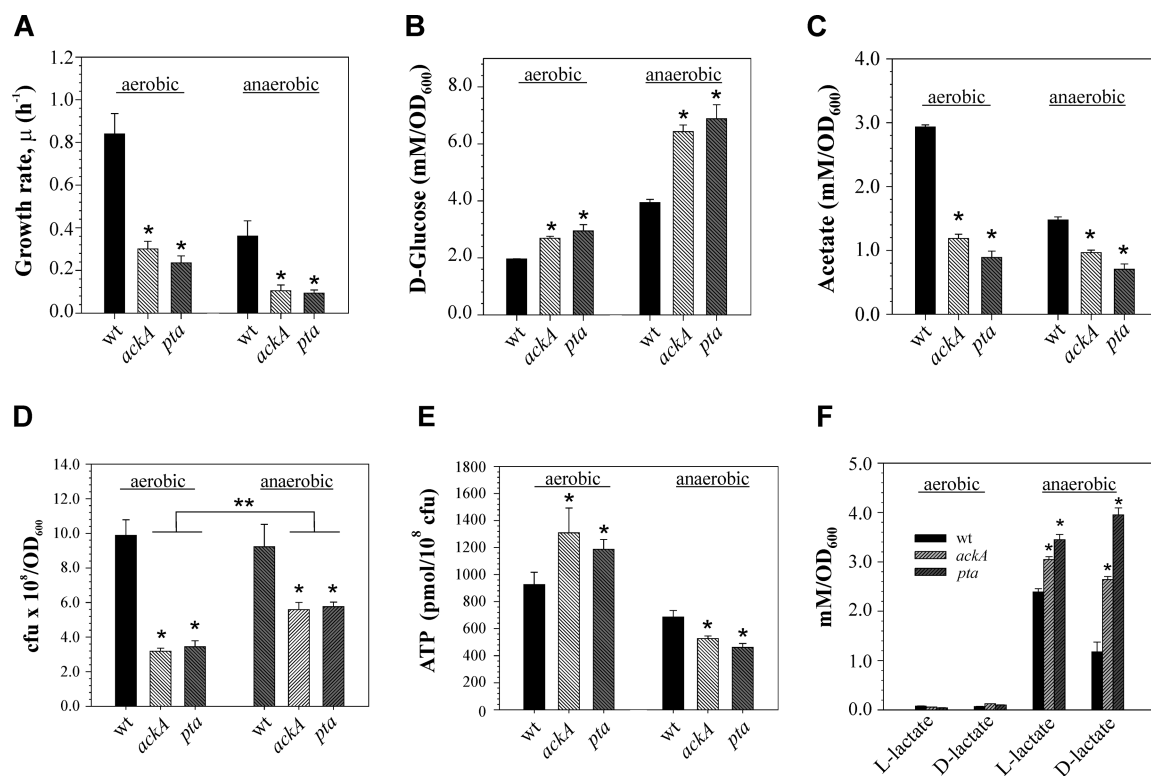


**Figure 1.** Inactivation of the Pta-AckA pathway affects growth characteristics and alters viability and energy status of *S. aureus* during aerobic and anaerobic growth. (A) Growth rate  $\mu$  ( $\text{hour}^{-1}$ ) of the wild-type strain UAMS-1 and mutant strains UAMS-1-*ackA* and UAMS-1-*pta* grown aerobically or anaerobically in TSB containing 0.25% glucose determined after 3 h of growth. (B) The concentrations of glucose consumed from the culture medium per OD<sub>600</sub> determined for strains UAMS-1, UAMS-1-*ackA*, and UAMS-1-*pta* after 3 h of growth. (C) The concentrations of accumulated acetic acid in the culture medium per OD<sub>600</sub> determined for strains UAMS-1, UAMS-1-*ackA*, and UAMS-1-*pta* after 3 h of growth. (D) Number of viable cells per OD<sub>600</sub> unit determined for strains UAMS-1, UAMS-1-*ackA*, and UAMS-1-*pta* after 3 h of growth. (E) Intracellular ATP concentrations determined for strains UAMS-1, UAMS-1-*ackA*, and UAMS-1-*pta* after 3 h of growth. (F) The concentrations of accumulated D- and L-lactic acids in the culture medium per OD<sub>600</sub> determined for strains UAMS-1, UAMS-1-*ackA*, and UAMS-1-*pta* after 3 h of growth. The results are presented as the means plus standard errors of the mean of duplicate determinations for at least three independent experiments. Statistical significance between the wild-type strain and *pta* and *ackA* mutants (\*) and *pta* and *ackA* mutants grown aerobically and anaerobically (\*\*) was determined by Student's *t* test ( $P \leq 0.001$ ).

chemical shifts were submitted to the Human Metabolome Database (HMDB)<sup>25</sup> and the Platform for RIKEN Metabolomics PRIME<sup>26</sup> for metabolite identification. An error tolerance of 0.08 and 0.25 ppm, for <sup>1</sup>H and <sup>13</sup>C, respectively, was used to assign the metabolites.

#### Relative Metabolite Concentration Changes

2D <sup>1</sup>H-<sup>13</sup>C HSQC NMR spectra were used to measure relative metabolite concentration changes by comparing HSQC peak intensities between spectra collected for the wild-type strain UAMS-1 and the mutant strains UAMS-1-*ackA* and UAMS-1-*pta*. The calculation of relative metabolite concentration changes was performed as described previously.<sup>13,14</sup> Briefly, a 2D <sup>1</sup>H-<sup>13</sup>C HSQC NMR spectrum was collected for each of the three biological replicates obtained for each group (e.g., UAMS-1). The 2D <sup>1</sup>H-<sup>13</sup>C HSQC spectra were all referenced to TMS-D<sub>4</sub>. Each individual 2D <sup>1</sup>H-<sup>13</sup>C HSQC NMR spectrum was then normalized to the sum of peak intensities for that specific spectrum. The peak intensities were then scaled, from 1 to 100, across the entire HSQC data set for each individual peak (e.g., ATP HSQC peak: <sup>13</sup>C 98.6 ppm, <sup>1</sup>H 6.10 ppm). An average peak intensity was calculated for each of these HSQC peaks per group. If multiple HSQC peaks were assigned to a single metabolite, then an average of all the HSQC peaks assigned to a metabolite were reported. A paired

Student's *t* test was utilized to determine the statistical significance of metabolite concentration changes between aerobic and anaerobic growth conditions.

## RESULTS

### Anaerobic Fermentation Partially Restores Viability of the *pta* and *ackA* Mutants

Growth of the *pta* and *ackA* mutants under anaerobic (fermentative) conditions provided an important basis for understanding the physiological defects associated with inactivation of the Pta-AckA pathway. Similar to their aerobic growth characteristics, fermentation by both *pta* and *ackA* mutants was accompanied by impaired growth rates (Figures 1A and S1), decreased acidification (Figure S1), and a reduction in the levels of excreted acetate relative to the wild-type strain (Figures 1C and S1). Furthermore, an increase in glucose uptake from the culture media was also evident for both the *pta* and *ackA* mutants under aerobic and fermentative growth (Figure 1B). However, surprisingly, both the *pta* and *ackA* mutants exhibited a partial restoration of viability (increase in colony-forming units (cfu) per unit OD<sub>600</sub>) relative to the wild-type strain under fermentative conditions (Figure 1D) despite a decrease in their intracellular ATP levels (Figure 1E). These observations not only suggest a role for

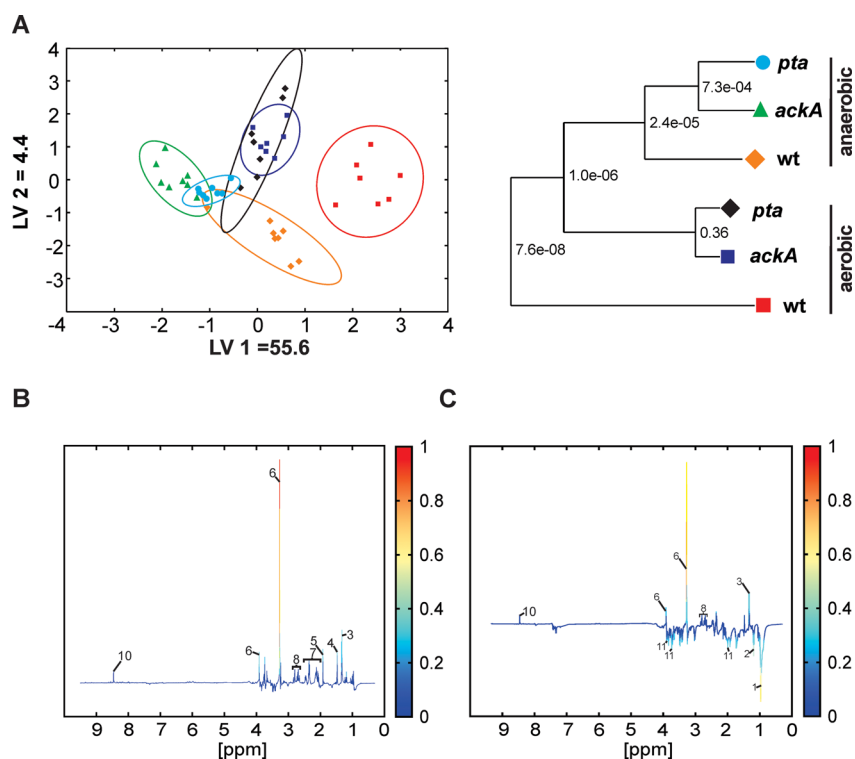


**Figure 2.** Disruption of the Pta-AckA pathway has a relatively smaller impact on *S. aureus* metabolome during anaerobiosis. (A) 2D LDA scores plots comparing the metabolic fingerprints of aerobically grown wild-type (red), UAMS-1-*ackA* (purple), and UAMS-1-*pta* (black) vs anaerobically grown wild-type (yellow), UAMS-1-*ackA* (green), and UAMS-1-*pta* (cyan). Dendrogram was generated from PCA scores using a Mahalanobis distance matrix with  $p$  values for the null hypothesis reported at each node. (B,C) OPLS-DA back-scaled loadings plot comparing anaerobically grown UAMS-1-*pta* (B) and UAMS-1-*ackA* (D) vs UAMS-1 wild-type strain. Peak intensities reflect the contribution of that peak to class separation, an up orientation represents a metabolite increased under anaerobic growth, and, conversely, a down orientation represents a metabolite increased under aerobic growth. The coloring of the back-scaled loadings plot is based on the scale factor applied during variable scaling prior to model training. Metabolite labels correspond to (1) branched chain amino acids (valine, isoleucine, leucine), (2) ethanol, (3) lactate, (4) alanine, (5) acetate, (6) betaine, (7) glutamate, (8) aspartate, (9) glycerol, (10) formate, and (11) homoserine.

fermentative metabolism in increasing survival of the *pta* and *ackA* mutants but also discount perturbations in intracellular ATP as a source of the observed differences in viability of these mutants. Although both aerobic and anaerobic fermentation resulted in poor growth of the *pta* and *ackA* mutants, only the latter fermentative growth conditions led to restoration of cell viability (Figure 1D). This suggests that the relative decrease in growth rate exhibited by the *pta* and *ackA* mutants to that of the wild-type strain does not result from increased cell death following inactivation of the Pta-AckA pathway.

#### Restoration of Redox Homeostasis in the *pta* and *ackA* Mutants under Fermentative Conditions

To further address the differences in viability observed under different oxygen tensions, we utilized 1D  $^1\text{H}$  NMR to compare the exponential-phase metabolomes of the *pta* and *ackA* mutants to its isogenic wild-type strain grown under both aerobic and fermentative conditions. Following acquisition of the 1D  $^1\text{H}$  NMR spectra, the table of integrals was used for principal component analysis (PCA). Although the PCA showed significant separation between the wild-type strain and corresponding *pta* and *ackA* mutants under both aerobic and fermentative conditions, a less-pronounced separation was observed following fermentation, suggesting that fermentative metabolism (as opposed to aerobic metabolism) may be less prone to perturbations associated with inactivation of the Pta-AckA pathway (Figure 2A). We reasoned that metabolic compensations in the *pta* and *ackA* mutants relative to the wild-

type strain may have augmented its survival during fermentation. To identify these metabolic differences, we performed orthogonal partial least-squares discriminant analysis (OPLS-DA), which relies on class membership, where the variation between classes are represented in the predictive component on the X-axis (Pp), and all other variations are represented in the orthogonal component Y-axis (Po). Multiple metabolites including branched-chain amino acids (valine, isoleucine, leucine), ethanol, lactate, alanine, acetate, betaine, glutamate, aspartate, glycerol, formate, and homoserine allowed discrimination of the *pta* and *ackA* mutant metabolomes from that of their isogenic wild-type strain under fermentative conditions (Figure 2B,C). However, among these metabolites, only lactate, betaine, formate, and aspartate appeared to be common to and in excess in both *pta* and *ackA* mutants relative to the wild-type strain (Figure 2B and C). Although these latter metabolites appear to be unrelated, metabolic pathways involved in their biosynthesis or degradation are potential contributors to cellular redox status during fermentation.

To validate any effects cellular redox status may have on cell viability of the *pta* and *ackA* mutants, we next tracked metabolic changes within these mutants by 2D  $^1\text{H}$ - $^{13}\text{C}$  HSQC NMR following supplementation of the media with labeled  $^{13}\text{C}_6$  glucose (see the Materials and Methods section). Exponentially growing bacteria were collected and used in the 2D  $^1\text{H}$ - $^{13}\text{C}$  HSQC NMR experiments to identify metabolic changes associated with inactivation of the Pta-AckA pathway during



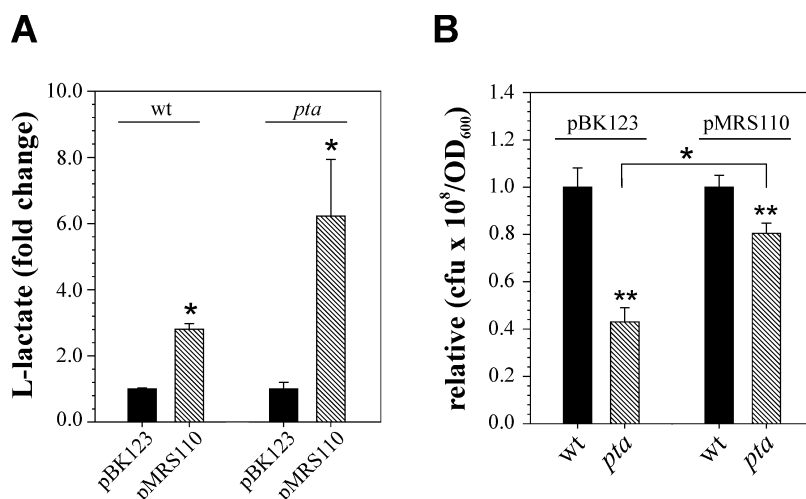


**Figure 4.** Overexpression of the *ldh1* gene attenuates negative impact on viability of the *pta* mutant during aerobic growth. (A) Relative concentrations of accumulated L-lactic acid in the culture medium per OD<sub>600</sub> determined for strains UAMS-1, UAMS-1-*ackA*, and UAMS-1-*pta* containing vector plasmid (pBK123) or *ldh1* expressing plasmid (pMRS110) after 3 h of growth. (B) Relative number of viable cells per OD<sub>600</sub> unit determined for strains UAMS-1, UAMS-1-*ackA*, and UAMS-1-*pta* containing vector plasmid (pBK123) or *ldh1* expressing plasmid (pMRS110) after 3 h of growth. The results are presented as the means plus standard errors of the mean of duplicate determinations for at least three independent experiments. Statistical significance between strains containing vector plasmid (pBK123) and *ldh1* expressing plasmid (pMRS110) (A,B) and between the wild-type strain and *pta* and *ackA* mutants (B) was determined by Student's *t* test (\*, \*\*; *P* ≤ 0.001).

and *ackA* mutants that require increased turnover of NADH to NAD<sup>+</sup> to maintain redox homeostasis, this phenotype did not result from a lack of lactate production. Rather, we observed an increased excretion of both D- and L-lactate by the *pta* and *ackA* mutants relative to the wild-type strain, suggesting that the decreased intracellular levels of lactate reflected increased turnover and export of carbon through the lactate dehydrogenase pathway in these mutants (Figure 1F). Collectively, these results indicate that achieving redox homeostasis may be crucial to increasing viability of the *pta* and *ackA* mutants.

#### Overexpression of the L-Lactate Dehydrogenase (Ldh1) Increase of Viability of the *pta* Mutant during Aerobic Growth

Given that the increased activation of fermentative pathways (D- and L-lactate) during anaerobiosis potentially allows *S. aureus* *pta* and *ackA* mutants to maintain redox homeostasis and viability, we argued that a similar correction of the redox status following inactivation of the Pta-AckA pathway under aerobic growth should prevent cell death. To test this hypothesis, we introduced a plasmid overexpressing L-lactate dehydrogenase (pMRS110) into the wild-type strain and the *pta* mutant and monitored cell viability and L-lactate production during aerobic growth. As expected, overexpression of the *ldh1* gene caused a significant increase in the excretion of L-lactate for both the wild-type strain and *pta* mutant (Figure 4A). However, excreted L-lactate concentrations in the media were higher for the *pta* mutant than the wild-type strain (Figure 4A), presumably due to increased glycolytic flux associated with disruption of the Pta-AckA pathway. More importantly, although pMRS110 mediated overexpression of the *ldh1* increased viability of the *pta* mutant relative to the control strain (*pta* mutant bearing vector control, pBK123), no differences in the viable cell counts were observed for the wild-type strain carrying either of these plasmids (Figure 4B). Overall, these results demonstrate that restoration of redox homeostasis can significantly attenuate the negative impact on cell viability associated with inactivation of the Pta-AckA pathway under aerobic growth conditions.

#### DISCUSSION

During aerobic growth in media containing glucose, when carbon flux toward the TCA cycle is limited due to carbon catabolite repression,<sup>33–37</sup> *S. aureus* primarily generates acetate by means of the Pta-AckA pathway, a phenomenon known as “acetate overflow”.<sup>10,30,32,38,39</sup> We have previously shown that under these conditions, the Pta-AckA pathway plays an indispensable role in maintenance of *S. aureus* fitness, as its inactivation results in growth defects and cell death. Although the precise reasons for the observed defects in growth and viability of *pta* and *ackA* mutants are not clearly understood, a role for ATP production (a byproduct of the Pta-AckA pathway) was ruled out earlier.<sup>10</sup> Interestingly, similar observations were also noted in other bacteria (i.e., it was shown that disruption of the *pta* gene in *Escherichia coli*<sup>40</sup> and inactivation of the *ackA* gene in *Streptococcus mutans*<sup>41</sup> did not cause a substantial loss in the amounts of generated ATP).

How do the *S. aureus* *pta* and *ackA* mutants compensate for the loss of ATP following inactivation of the Pta-AckA pathway? The results of the current study suggest that disruption of this pathway under aerobic conditions increases glycolytic flux and redirects carbon toward the TCA cycle. This was reflected by a higher glucose consumption rate and by increased intracellular concentrations of glycolytic and TCA cycle intermediates. Additionally, transcriptional upregulation of key glycolytic and TCA cycle genes (i.e., *pfkA* and *citZ*) was also observed in the *pta* and *ackA* mutants.<sup>10</sup> A similar increase in the expression of both TCA cycle and central glycolytic enzymes in the Pta-AckA pathway mutants was reported for *E. coli*.<sup>42,43</sup> An increase in carbon flux through both glycolysis and the TCA cycle could compensate for ATP loss following inactivation of the Pta-AckA pathway because sufficient reducing equivalents generated through these pathways will be converted to ATP by means of oxidative phosphorylation.<sup>44</sup> In support of this argument, both respiration rates and intracellular NAD<sup>+</sup> and NADH concentrations were observed to be significantly higher in the *pta* and *ackA* mutants.<sup>10</sup>

Both NAD<sup>+</sup> and NADH are the primary determinants of redox balance in living cells and their intracellular concentrations are crucial for the sustained function of a variety of metabolic pathways. Hence, any compensatory increase in flux through glycolysis and TCA cycle raises the potential risk of a redox imbalance in cells. Indeed, we speculated that the altered redox environment associated with the *pta* and *ackA* mutations might contribute to the observed growth and viability defects in these mutants. Evidence supporting this notion was observed when reduced viability, a characteristic of both *pta* and *ackA* mutant populations, was partially restored to wild-type levels following growth under fermentative conditions. Fermentation by *pta* and *ackA* mutants not only prevented redirection of carbon toward the TCA cycle (as this pathway is inactive under anoxic conditions) but apparently also resulted in a balanced intracellular turnover of NADH to NAD<sup>+</sup>. NMR metabolomics analysis and metabolite excretion profiles of anaerobically grown *pta* and *ackA* mutants identified multiple possibilities that could aid in the turnover of intracellular pools of NADH and NAD<sup>+</sup> in these mutants. Specifically, whereas biosynthesis of betaine from betaine aldehyde and aspartate from glutamate would result in the generation of NADH, the conversion of pyruvate to lactate increases turnover of NADH to NAD<sup>+</sup>. Similarly, excess levels of formate in the cells may be indicative of decreased formate dehydrogenase activity, an adaptive strategy that could potentially limit excess NADH production from NAD<sup>+</sup>. These observations broadly correlate activity of reactions that augment cellular redox homeostasis to increased viability of the *pta* and *ackA* mutants under fermentative conditions.

Confirmatory evidence linking the altered intracellular redox status and decreased viability following inactivation of the Pta-AckA pathway could be established only after overexpressing L-lactate dehydrogenase in the *S. aureus pta* mutant. *S. aureus* possesses two L-lactate dehydrogenases (Ldh1/2) and two D-lactate dehydrogenases (SACOL2535 and SACOL2574).<sup>30,45,46</sup> However, these enzymes are generally not active under aerobic conditions.<sup>31</sup> Overexpression of *ldh1* in the *pta* mutant using an inducible promoter partially restored its viability to wild-type levels under aerobic conditions. Interestingly, this approach did not restore the decreased growth rate of the *pta* mutant (data not shown), suggesting redox-independent regulation of growth following inactivation of the Pta-AckA pathway. An alternate possibility is that restoration of redox homeostasis in the *pta* mutant by overexpression of *ldh1* may decrease the intracellular pools of ATP leading to defects in growth rate.

In conclusion, it has often been argued that in glucose-rich environments, carbon flux through the Pta-AckA pathway is a rapid means by which *S. aureus* generates ATP to support fast growth under aerobic conditions. Although this may be true in principle, our data clearly suggests that the Pta-AckA pathway may have an alternate role in maintaining redox homeostasis by diverting carbon away from the TCA cycle. The inability to achieve this balance results in growth defects and cell death due to redox toxicity. Given that multiple bacterial species not only possess the Pta-AckA pathway but also exhibit similar physiological phenotypes following its inactivation, we argue that the ability to maintain redox homeostasis by directing carbon through the Pta-AckA pathway may be a universal phenomenon.

## ■ ASSOCIATED CONTENT

### 📄 Supporting Information

The Supporting Information is available free of charge on the ACS Publications website at DOI: 10.1021/acs.jproteome.5b01089.

Supplementary figures demonstrating inactivation of the Pta-AckA pathway impairs growth of *S. aureus* and overlay of 2D <sup>1</sup>H–<sup>13</sup>C HSQC spectra generated from *S. aureus* UAMS-1 metabolite extracts. A table showing relative metabolite concentrations for all strains under aerobic or fermentation conditions. (PDF)

## ■ AUTHOR INFORMATION

### Corresponding Author

\*Phone: (402) 472-3039; fax: (402) 472-9402; e-mail: rpowers3@unl.edu.

### Author Contributions

D.D.M. and M.R.S. contributed equally to this work. D.D.M., M.R.S., V.C.T., R.P., and K.W.B. designed the experiments, analyzed the data, and wrote the manuscript; D.D.M., M.R.S., and V.C.T. performed the experiments.

### Notes

The authors declare no competing financial interest.

## ■ ACKNOWLEDGMENTS

This manuscript was supported by National Institute of Health grants P30 GM103335 (R.P.), P01-AI083211 (K.W.B.), R01-AI038901 (K.W.B.), and from the American Heart Association grant 0860033Z (R.P.). Parts of this research were performed in facilities renovated with support from the National Institutes of Health (RR015468-01).

## ■ REFERENCES

- (1) Lowy, F. D. Staphylococcus aureus infections. *N. Engl. J. Med.* **1998**, *339* (8), 520–32.
- (2) Chambers, H. F.; Deleo, F. R. Waves of resistance: Staphylococcus aureus in the antibiotic era. *Nat. Rev. Microbiol.* **2009**, *7* (9), 629–41.
- (3) Wertheim, H. F.; Vos, M. C.; Ott, A.; van Belkum, A.; Voss, A.; Kluytmans, J. A.; van Keulen, P. H.; Vandenbroucke-Grauls, C. M.; Meester, M. H.; Verbrugh, H. A. Risk and outcome of nosocomial Staphylococcus aureus bacteraemia in nasal carriers versus non-carriers. *Lancet* **2004**, *364* (9435), 703–5.
- (4) Novick, R. P. Autoinduction and signal transduction in the regulation of staphylococcal virulence. *Mol. Microbiol.* **2003**, *48* (6), 1429–49.
- (5) Seidl, K.; Stucki, M.; Rugg, M.; Goerke, C.; Wolz, C.; Harris, L.; Berger-Bachi, B.; Bischoff, M. Staphylococcus aureus CcpA affects virulence determinant production and antibiotic resistance. *Antimicrob. Agents Chemother.* **2006**, *50* (4), 1183–94.
- (6) Majerczyk, C. D.; Sadykov, M. R.; Luong, T. T.; Lee, C.; Somerville, G. A.; Sonenshein, A. L. Staphylococcus aureus CodY negatively regulates virulence gene expression. *J. Bacteriol.* **2008**, *190* (7), 2257–65.
- (7) Chaffin, D. O.; Taylor, D.; Skerrett, S. J.; Rubens, C. E. Changes in the Staphylococcus aureus transcriptome during early adaptation to the lung. *PLoS One* **2012**, *7* (8), e41329.
- (8) Cheung, A. L.; Bayer, A. S.; Zhang, G.; Gresham, H.; Xiong, Y. Q. Regulation of virulence determinants in vitro and in vivo in Staphylococcus aureus. *FEMS Immunol. Med. Microbiol.* **2004**, *40* (1), 1–9.
- (9) Richardson, A. R.; Somerville, G. A.; Sonenshein, A. L., Regulating the Intersection of Metabolism and Pathogenesis in

Gram-positive Bacteria. *Microbiol Spectr* **2015**, *3* (3), 12910.1128/microbiolspec.MBP-0004-2014

(10) Sadykov, M. R.; Thomas, V. C.; Marshall, D. D.; Wenstrom, C. J.; Moormeier, D. E.; Widhelm, T. J.; Nuxoll, A. S.; Powers, R.; Bayles, K. W. Inactivation of the Pta-AckA pathway causes cell death in *Staphylococcus aureus*. *J. Bacteriol.* **2013**, *195* (13), 3035–44.

(11) Sharma-Kuinkel, B. K.; Mann, E. E.; Ahn, J. S.; Kuechenmeister, L. J.; Dunman, P. M.; Bayles, K. W. The *Staphylococcus aureus* LytSR two-component regulatory system affects biofilm formation. *J. Bacteriol.* **2009**, *191* (15), 4767–75.

(12) Meyer, H.; Liebeke, M.; Lalk, M. A protocol for the investigation of the intracellular *Staphylococcus aureus* metabolome. *Anal. Biochem.* **2010**, *401* (2), 250–259.

(13) Halouska, S.; Zhang, B.; Gaupp, R.; Lei, S.; Snell, E.; Fenton, R. J.; Barletta, R. G.; Somerville, G. A.; Powers, R. Revisiting Protocols for the NMR Analysis of Bacterial Metabolomes. *J. Integr OMICS* **2013**, *3* (2), 120–137.

(14) Zhang, B.; Halouska, S.; Schiaffo, C. E.; Sadykov, M. R.; Somerville, G. A.; Powers, R. NMR analysis of a stress response metabolic signaling network. *J. Proteome Res.* **2011**, *10* (8), 3743–54.

(15) Simpson, A. J.; Brown, S. A. Purge NMR: effective and easy solvent suppression. *J. Magn. Reson.* **2005**, *175* (2), 340–6.

(16) Delaglio, F.; Grzesiek, S.; Vuister, G. W.; Zhu, G.; Pfeifer, J.; Bax, A. NMRPipe: a multidimensional spectral processing system based on UNIX pipes. *J. Biomol. NMR* **1995**, *6* (3), 277–93.

(17) Johnson, B. A. Using NMRView to visualize and analyze the NMR spectra of macromolecules. *Methods Mol. Biol.* **2004**, *278*, 313–52.

(18) Worley, B.; Powers, R. MVAPACK: a complete data handling package for NMR metabolomics. *ACS Chem. Biol.* **2014**, *9* (5), 1138–44.

(19) Worley, B.; Powers, R. Simultaneous Phase and Scatter Correction for NMR Datasets. *Chemom. Intell. Lab. Syst.* **2014**, *131*, 1–6.

(20) De Meyer, T.; Sinnaeve, D.; Van Gasse, B.; Tshiporkova, E.; Rietzschel, E. R.; De Buyzere, M. L.; Gillebert, T. C.; Bekaert, S.; Martins, J. C.; Van Criekeing, W. NMR-based characterization of metabolic alterations in hypertension using an adaptive, intelligent binning algorithm. *Anal. Chem.* **2008**, *80* (10), 3783–90.

(21) Halouska, S.; Powers, R. Negative impact of noise on the principal component analysis of NMR data. *J. Magn. Reson.* **2006**, *178* (1), 88–95.

(22) Savorani, F.; Tomasi, G.; Engelsen, S. B. icoshift: A versatile tool for the rapid alignment of 1D NMR spectra. *J. Magn. Reson.* **2010**, *202* (2), 190–202.

(23) Xu, Q.-S.; Liang, Y.-Z.; Du, Y.-P. Monte Carlo cross-validation for selecting a model and estimating the prediction error in multivariate calibration. *J. Chemom.* **2004**, *18*, 112–120.

(24) Eriksson, L.; Trygg, J.; Wold, S. CV-ANOVA for significance testing of PLS and OPLS® models. *J. Chemom.* **2008**, *22*, 594–600.

(25) Wishart, D. S.; Jewison, T.; Guo, A. C.; Wilson, M.; Knox, C.; Liu, Y.; Djoumbou, Y.; Mandal, R.; Aziat, F.; Dong, E.; Bouatra, S.; Sinelnikov, I.; Arndt, D.; Xia, J.; Liu, P.; Yallou, F.; Bjorn Dahl, T.; Perez-Pineiro, R.; Eisner, R.; Allen, F.; Neveu, V.; Greiner, R.; Scalbert, A. HMDB 3.0—The Human Metabolome Database in 2013. *Nucleic Acids Res.* **2013**, *41*, D801–D807.

(26) Akiyama, K.; Chikayama, E.; Yuasa, H.; Shimada, Y.; Tohge, T.; Shinozaki, K.; Hirai, M. Y.; Sakurai, T.; Kikuchi, J.; Saito, K. PRIME: a Web site that assembles tools for metabolomics and transcriptomics. *In Silico Biol.* **2008**, *8* (3–4), 339–45.

(27) Garvie, E. I. Bacterial lactate dehydrogenases. *Microbiol Rev.* **1980**, *44* (1), 106–39.

(28) Ojima, Y.; Suryadarma, P.; Tsuchida, K.; Taya, M. Accumulation of pyruvate by changing the redox status in *Escherichia coli*. *Biotechnol. Lett.* **2012**, *34* (5), 889–93.

(29) Sun, J. L.; Zhang, S. K.; Chen, J. Y.; Han, B. Z. Metabolic profiling of *Staphylococcus aureus* cultivated under aerobic and anaerobic conditions with (1)H NMR-based nontargeted analysis. *Can. J. Microbiol.* **2012**, *58* (6), 709–18.

(30) Ferreira, M. T.; Manso, A. S.; Gaspar, P.; Pinho, M. G.; Neves, A. R. Effect of oxygen on glucose metabolism: utilization of lactate in *Staphylococcus aureus* as revealed by in vivo NMR studies. *PLoS One* **2013**, *8* (3), e58277.

(31) Fuchs, S.; Pane-Farre, J.; Kohler, C.; Hecker, M.; Engelmann, S. Anaerobic gene expression in *Staphylococcus aureus*. *J. Bacteriol.* **2007**, *189* (11), 4275–89.

(32) Ledala, N.; Zhang, B.; Seravalli, J.; Powers, R.; Somerville, G. A. Influence of iron and aeration on *Staphylococcus aureus* growth, metabolism, and transcription. *J. Bacteriol.* **2014**, *196* (12), 2178–89.

(33) Crabtree, H. G. Observations on the carbohydrate metabolism of tumours. *Biochem. J.* **1929**, *23* (3), 536–45.

(34) Sonenshein, A. L. Control of key metabolic intersections in *Bacillus subtilis*. *Nat. Rev. Microbiol.* **2007**, *5* (12), 917–27.

(35) Seidl, K.; Muller, S.; Francois, P.; Kriebitzsch, C.; Schrenzel, J.; Engelmann, S.; Bischoff, M.; Berger-Bachi, B. Effect of a glucose impulse on the CcpA regulon in *Staphylococcus aureus*. *BMC Microbiol.* **2009**, *9*, 95.

(36) Sadykov, M. R.; Hartmann, T.; Mattes, T. A.; Hiatt, M.; Jann, N. J.; Zhu, Y.; Ledala, N.; Landmann, R.; Herrmann, M.; Rohde, H.; Bischoff, M.; Somerville, G. A. CcpA coordinates central metabolism and biofilm formation in *Staphylococcus epidermidis*. *Microbiology* **2011**, *157* (12), 3458–3468.

(37) Hanson, R. S.; Cox, D. P. Effect of different nutritional conditions on the synthesis of tricarboxylic acid cycle enzymes. *J. Bacteriol.* **1967**, *93* (6), 1777–87.

(38) Majewski, R. A.; Domach, M. M. Simple constrained-optimization view of acetate overflow in *E. coli*. *Biotechnol. Bioeng.* **1990**, *35* (7), 732–8.

(39) Somerville, G. A.; Proctor, R. A. At the crossroads of bacterial metabolism and virulence factor synthesis in *Staphylococci*. *Microbiol Mol. Biol. Rev.* **2009**, *73* (2), 233–48.

(40) Chang, D. E.; Shin, S.; Rhee, J. S.; Pan, J. G. Acetate metabolism in a pta mutant of *Escherichia coli* W3110: importance of maintaining acetyl coenzyme A flux for growth and survival. *J. Bacteriol.* **1999**, *181* (21), 6656–63.

(41) Kim, J. N.; Ahn, S. J.; Burne, R. A. Genetics and Physiology of Acetate Metabolism by the Pta-Ack Pathway of *Streptococcus mutans*. *Appl. Environ. Microbiol.* **2015**, *81* (15), 5015–25.

(42) Wolfe, A. J.; Chang, D. E.; Walker, J. D.; Seitz-Partridge, J. E.; Vidaurri, M. D.; Lange, C. F.; Pruss, B. M.; Henk, M. C.; Larkin, J. C.; Conway, T. Evidence that acetyl phosphate functions as a global signal during biofilm development. *Mol. Microbiol.* **2003**, *48* (4), 977–88.

(43) Wolfe, A. J. The acetate switch. *Microbiol Mol. Biol. Rev.* **2005**, *69* (1), 12–50.

(44) Mitchell, P.; Moyle, J. Chemiosmotic hypothesis of oxidative phosphorylation. *Nature* **1967**, *213* (5072), 137–9.

(45) Stockland, A. E.; San Clemente, C. L. Multiple forms of lactate dehydrogenase in *Staphylococcus aureus*. *J. Bacteriol.* **1969**, *100* (1), 347–53.

(46) Boyle-Vavra, S.; de Jonge, B. L.; Ebert, C. C.; Daum, R. S. Cloning of the *Staphylococcus aureus* ddh gene encoding NAD<sup>+</sup>-dependent D-lactate dehydrogenase and insertional inactivation in a glycopeptide-resistant isolate. *J. Bacteriol.* **1997**, *179* (21), 6756–63.